Bias-Dependent Stability of Perovskite Solar Cells Studied Using Natural and Concentrated Sunlight

Anoop K. M., Mark V. Khenkin, Francesco Di Giacomo, Yulia Galagan, Stav Rahmany, Lioz Etgar, Eugene A. Katz, and Iris Visoly-Fisher*

Degradation rates in perovskite solar cells (PSCs) were previously shown to be bias dependent; however, little is known about the mechanisms and driving factors that account for such degradation. Herein, stability studies under concentrated sunlight are demonstrated as a powerful experimental methodology to investigate bias-dependent PSC degradation mechanisms. Stress testing of encapsulated PSCs' stability shows that light intensity is more significant than the illumination dose for PSC degradation under short-circuit (SC) conditions, whereas the dose is the determining factor under open-circuit (OC) stressing. This indicates that different degradation mechanisms are dominant under different bias conditions. It is postulated that degradation at SC biasing is dominated by ion migration, facilitated by photogenerated defects. Degradation at OC biasing can be explained by photogenerated radicals acting as nonradiative recombination centers (charge traps), which are created via reactions with accumulated charge carriers. Trap formation upon OC biasing is in accordance with degradation of photoluminescence and OC voltage (V_{OC}) observed under this stress. A combination of multiple mechanisms, all with reduced driving forces compared with OC/SC biasing, explains degradation at maximum power point biasing. Understanding the bias effect on PSC stability can elucidate the underlying degradation mechanisms and lead to routes to reduce them.

1. Introduction

Perovskite solar cells (PSCs) have emerged as a promising photovoltaic (PV) technology with high efficiency (up to 25.2% for a single-junction PSC[1]) and low fabrication costs. However, implementation of this technology is restricted by limited PSC stability.[2–6] The degradation of PSCs was found to depend on

multiple parameters, including visible and ultraviolet (UV) radiation, temperature,[7–9] atmospheric gases (oxygen, humidity),[10,11] and electrical bias.[6,12–15] The latter is of special importance, as PV cells always operate under bias, typically at their maximum power point (MPP). However, cell-to-cell-induced bias in module or tandem configuration may deviate from MPP, and shaded cells may even experience reverse bias imposed by connected illuminated cells in the module.[16] Understanding the bias effect on PSC stability can elucidate the underlying degradation mechanisms and eventually lead to routes for eliminating or reducing them.

Bias-dependent degradation rates of PSCs were noted in multiple publications,[10,12,14,15,17,18] indicating bias-affected degradation mechanisms, i.e., mechanisms that were triggered by bias application or triggered by other factors and accelerated by applied bias. However, understanding the mechanisms and driving factors that account for such degradation is still limited.[6,12–14] Herein, we study the effect of light intensity and cell temperature on PSC degradation at different bias conditions toward the better understanding of such mechanisms.

Bias-induced migration of charged defects was suggested to affect the net charge concentration at interfacial space charge regions in the perovskite layer, affecting photogenerated charge separation and collection.[8,13,14] Interlayer migration of charged species under bias can also affect the (opto)electronic properties

A. K. M., Dr. M. V. Khenkin, Prof. E. A. Katz, Prof. I. Visoly-Fisher
Department of Solar Energy and Environmental Physics
Swiss Institute for Dryland Environmental and Energy Research
Jacob Blaustein Institutes for Desert Research
Ben-Gurion University of the Negev
Midreshet Ben-Gurion 8499000, Israel
E-mail: irisvf@bgu.ac.il

Prof. E. A. Katz, Prof. I. Visoly-Fisher
Ilse Katz Institute for Nanoscale Science & Technology
Ben-Gurion University of the Negev
Be'er Sheva 8410501, Israel

The ORCID identification number(s) for the author(s) of this article can be found under https://doi.org/10.1002/solr.201900335.

Dr. F. Di Giacomo, Dr. Y. Galagan
TNO – Solliance
High Tech Campus, Eindhoven, The Netherlands

Dr. F. Di Giacomo
CHOSE (Centre for Hybrid and Organic Solar Energy)
Department of Electronic Engineering
University of Rome Tor Vergata
Rome 00133, Italy

S. Rahmany, Prof. L. Etgar
Casali Center for Applied Chemistry
Institute of Chemistry
Hebrew University of Jerusalem
Jerusalem 9190401, Israel

of various cell layers, hence its power conversion efficiency (PCE).[17,19–23] Bias-dependent trap charging will modify internal fields in the cell, affecting photocurrent collection.[15]

The interplay between illumination and bias with respect to degradation is of special importance, as this is the situation under normal cell operating conditions. Nie et al.[15] suggested photoinduced trap formation in $CH_3NH_3PbI_3$. Photogeneration of charged defects[15,24,25] will determine the magnitude of the effect of their bias-induced migration on the cell performance. A possible mechanism for such defect photogeneration is via weakening and breakage of chemical bonds by photogenerated charge carriers, which is especially severe under open circuit (OC) conditions.[12,26] Trap formation by interaction with photogenerated charge carriers was also suggested.[27] Exposure to atmospheric gases (oxygen, humidity) under light and bias will provide additional degradation pathways,[10,28,29] which can be excluded by careful cell encapsulation.

Recently, we speculated that a combination of degradation mechanisms, with possible changes in the dominating mechanism at different bias conditions, can account for bias-dependent degradation rates in PSCs.[13] We suggested that degradation at OC conditions is governed by trap charging combined with radical formation and interlayer ion diffusion, whereas at short circuit (SC) and maximum power point (MPP) conditions, ion migration within the perovskite layer is the dominant mechanism. Herein we describe experimental studies of the combined effect of light, temperature, and bias on PSCs' stability and degradation, to examine this hypothesis.

Toward that end, PSC stressing was applied under different combinations of bias (OC, SC, and MPP) and illumination intensities afforded by concentrated natural sunlight,[30] and the changes in PSC photovoltaic performance were followed. Sunlight concentration allows accelerated stability studies and studying the effect of light intensity on cell degradation. Our experimental methodology allows independent control of sunlight intensity, the sample temperature, and environment during the exposure, as detailed in previous studies[31,32] and Experimental Section. Elevated illumination intensities were scarcely used before to study performance and stability of certain PSCs.[33,34] Herein, we show a systematic study of the combined effect of bias and light intensity on PSC degradation. The use of concentrated natural sunlight implies conditions relevant for standard cell operation and provides insights into the light-bias-induced degradation mechanisms in PSCs.

2. Results

Mixed cation, mixed halide perovskite-based cells (ITO/ SnO_2/ $Cs_{0.15}(CH(NH_2)_2)_{0.85}PbI_{2.75}Br_{0.25}$/ Spiro-OMeTAD/ Au, "Cell 1") were carefully encapsulated to eliminate the effects of atmospheric gases and exposed to various sunlight concentrations at different biases, with their PV performances being followed periodically. Some measurements were repeated with similarly encapsulated but slightly different n-i-p PSCs from two manufacturing labs ("Cell 2" and "Cell 3"), to check the qualitative repeatability of the results and avoid cell type-specific conclusions (see Experimental Section for details and Supporting Information for repeated results). We note, however, that the

relevance of our results to p-i-n cells should be verified. Two different setups ("mini-dish" and "solar furnace") were used for sunlight concentration as described in Experimental Section. The systems differ in their temperature control schemes, which allowed separating the effect of light from the combined effect of light and temperature, as described later.

2.1. Stressing at OC versus SC: The Effect of Illumination Intensity

When stressing was performed at OC, initial fast PCE degradation was observed followed by the significantly slower one at all illumination intensities, as previously reported for PSCs.[12] Analyzing the normalized PCE variations at OC as a function of illuminating dose (intensity × exposure time) shows similar degradation patterns at different illumination intensities (**Figure 1**a and 2b, Figure S3a, Supporting Information), with the transition to the slower degradation stage occurring after 20%–40% PCE degradation with respect to its initial value. The initial PCE degradation rate in all cases was $4.3 +/- 1\%$/ (sun × hour). We therefore conclude that dose is the determining factor for PCE photodegradation at OC conditions.

Stressing under SC revealed again initial fast PCE decrease followed by significantly slower degradation. However, the extent of the initial degradation was found to be intensity dependent, with larger PCE degradation at larger sunlight concentrations (Figure 1b and 2c, Figure S3d, Supporting Information). We therefore conclude that light intensity is the determining factor for cell degradation at SC biasing, in contrast with the behavior observed for OC stressing. This difference points to different degradation mechanisms operating at different bias conditions.

2.2. Stressing at OC versus SC: The Combined Effect of Illumination Intensity and Temperature

Stressing experiments under OC and SC biasing were repeated using the "mini-dish" solar concentrator, where the cell temperatures gradually increase with increasing illumination intensity (Figure 2a), to examine the combined effect of illumination intensity and temperature. This is in contrast to the very small temperature variation with illumination intensity in the "solar furnace" concentrator used in studies shown in Figure 1 (see Figure 2a and Experimental Section). Elevated temperatures were previously found to accelerate PSC dark-[35,36] and photo-degradation.[12,32,37–39]

Despite the temperature increase with light intensity in this experiment, degradation at OC biasing was also dose dependent up to 20 suns illumination ($\approx$40 °C, Figure 2a and b, Figure S3a, Supporting Information) in agreement with the results obtained with insignificant temperature variations (Figure 1a). In this range, PCE degradation at OC biasing is due to decrease in V_{OC} and FF (Figure S1, Supporting Information). Further increase in illumination irradiance to 30 suns, 55 °C, leads to deviation from the observed pattern with a significantly accelerated PCE degradation rate accompanied by J_{SC} reduction (Figure 2a and Figure S1, Supporting Information). We therefore conclude that at a certain critical temperature, additional degradation process(es) kick in. Control experiments at 1 sun illumination and varying
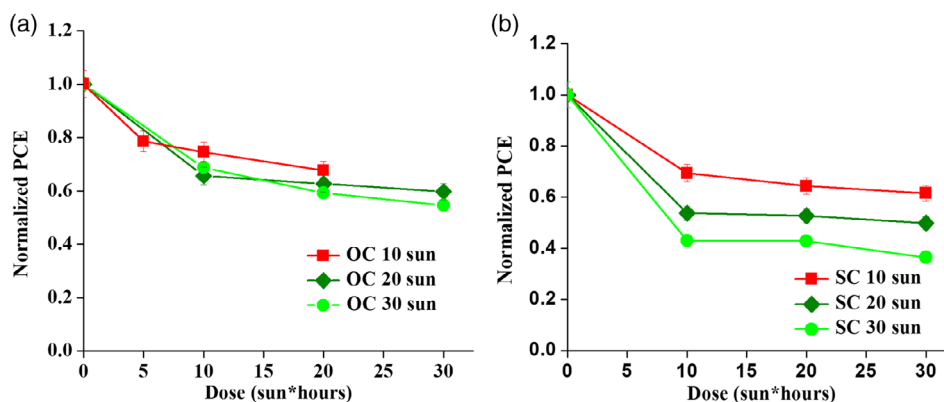
Figure 1. Normalized PCE variations (normalized to the initial PCE value) with sunlight exposure, indicated as dose (sunlight concentration × exposure time), of PSCs ("Cell 1") at a) OC and b) SC, using the "solar furnace" concentrator (see Experimental Section for details and initial cell performance). Irradiance of 1 sun is equal to $100\,mW\,cm^{-2}$. A dose of 1 sun × hour is equal to fluence of $360\,J\,cm^{-2}$.
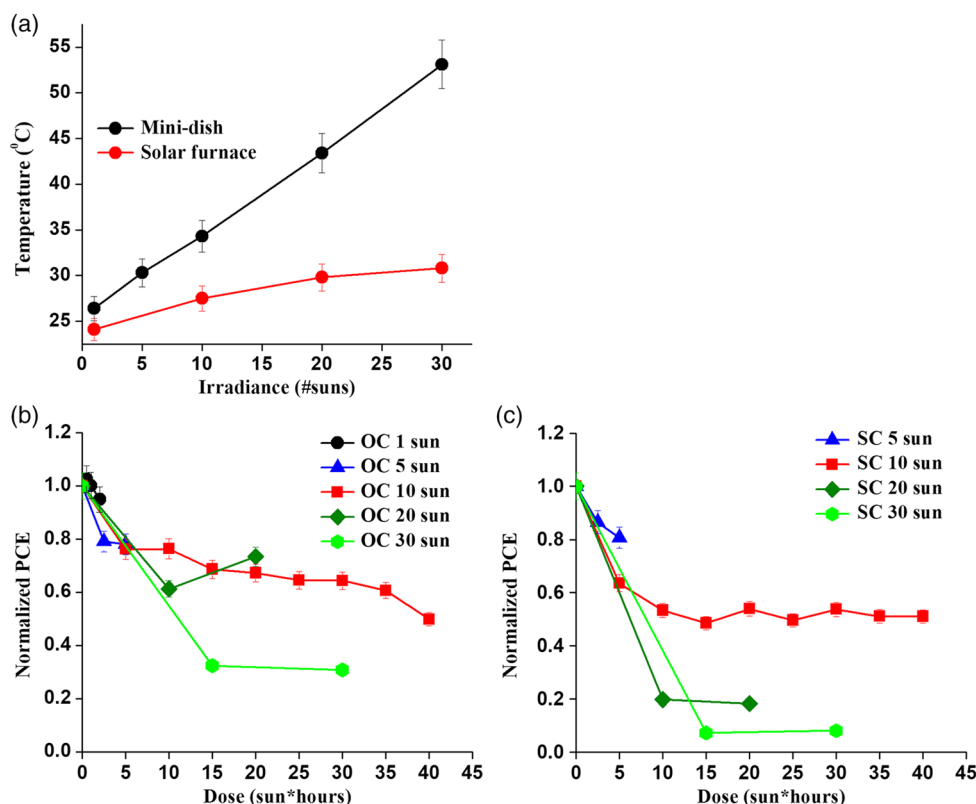

Figure 2. a) Cell temperature dependence on irradiance in the "mini-dish" and "solar furnace" sunlight concentrators. These systems differ in their temperature control schemes, as described in the Experimental Section. b,c) Normalized PCE variations with dose of PSCs ("Cell 1") at (b) OC biasing c) SC biasing using the "mini-dish" concentrator.

temperatures confirmed that elevated temperature beyond 40 °C can significantly accelerate the degradation at OC biasing (**Figure 3**a, Figure S4a, Supporting Information).

Analogous experiments of the combined effect of temperature and light intensity on degradation at SC biasing (Figure 2c, Figure S3b, Supporting Information) also revealed a pattern qualitatively similar to light-only-dependent SC stressing (Figure 1b) where the degradation was intensity dependent. However, all

the principal PV parameters (including J_{SC}) decrease simultaneously at SC stressing (Figure S2, Supporting Information). Compared with OC biasing, the temperature was found to have a less pronounced effect at SC biasing under 1 sun illumination (Figure 3 and Figure S4, Supporting Information). The degradation rate was accelerated under concentrated sunlight and elevated temperatures at all irradiance levels (Figure 2c compared with Figure 1b), making it difficult to separate a "critical" temperature
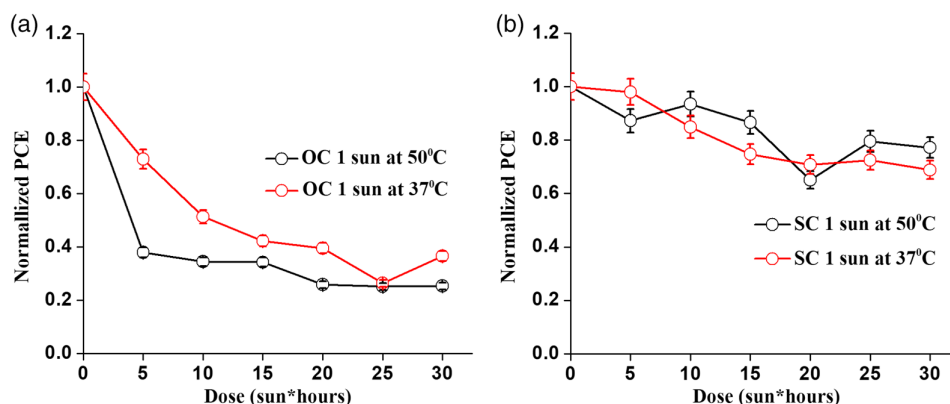
Figure 3. Normalized PCE variations with doses of PSCs ("Cell 1") at a) OC b) SC biasing for two distinct temperatures under one-sun-simulated illumination.

or/and light intensity corresponding to the onset of new degradation process(es) in analogy with the effect observed under OC biasing.

2.3. Stressing at Maximum Power Point (MPP)

Cell stressing at MPP showed slight PCE deterioration at sunlight concentrations up to 20 suns and significant degradation at 30 suns (cell temperature: 30–35 °C, **Figure 4**a,b), the latter with a pattern qualitatively similar to PCE degradation at OC at cell temperatures below 40 °C (initial degradation of 30% at rate 4.5%/sun × hour). Other PV parameters showed qualitatively similar behavior as that observed for PCE (Figure S5, Supporting Information). Temperature-dependent studies at MPP under one-sun-simulated illumination showed a temperature effect reminiscent of that at OC with stressing at 55 °C being significantly faster than that at 20 °C (Figure 4c).
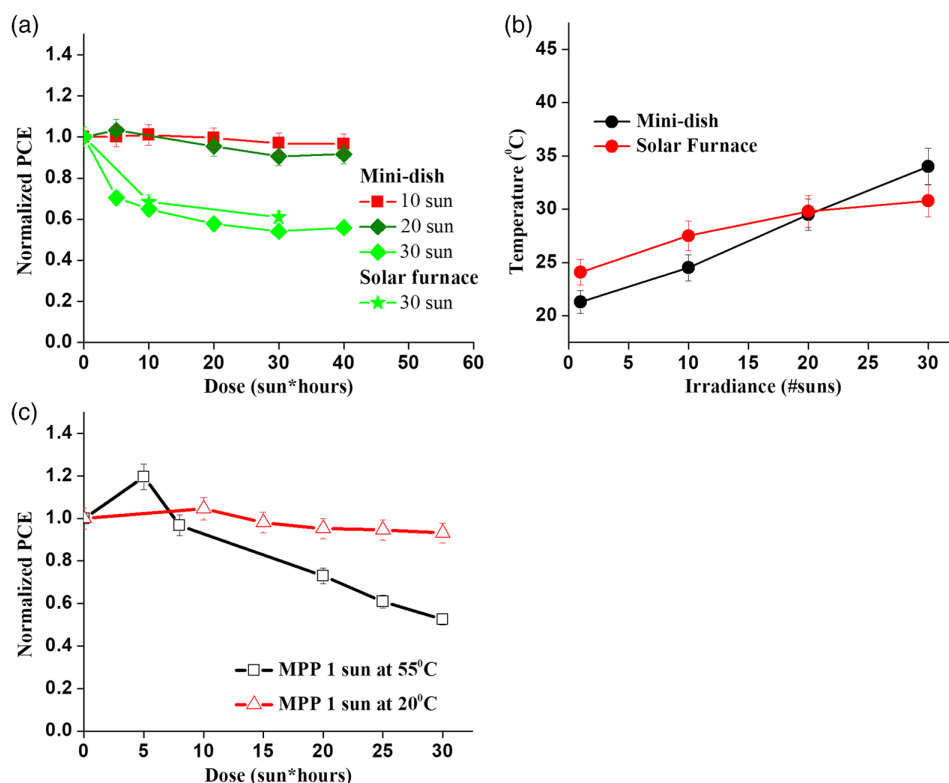

Figure 4. a) Normalized PCE variations with illumination dose of PSCs ("Cell 1") at MPP under different sunlight concentrations using the "mini-dish" and the "solar furnace" concentrators. b) Cell temperatures during stressing at MPP (for details on temperature control see Experimental Section). c) Normalized PCE variations with doses at MPP for two distinct temperatures under one-sun-simulated illumination ("Cell 2").

2.4. Outdoor Stressing

Stability characterization under outdoor exposure to natural sunlight was performed to relate the stability measured under concentrated sunlight to that at typical operating conditions. We note the differences between outdoor stressing and that under simulated one-sun illumination, due to diurnal variations in the sunlight intensity, spectrum, and cell temperature, as well as the daily light–dark cycling, allowing reversible cell performance dynamics. For a detailed discussion of recoverable versus nonrecoverable degradation and comparison of continuous and intermittent illumination effects on degradation, the reader is referred to our previous study[40].

Different degradation patterns at different bias conditions were demonstrated also by the outdoor stressing results: degradation at OC was faster than that at SC and MPP, in agreement with constant one-sun illumination studies described earlier (and summarized in Figure S6, Supporting Information). V_{oc} and FF degraded faster at OC biasing, whereas the overall J_{sc} degradation was almost similar under all bias conditions (**Figure 5** and Figure S7, Supporting Information).

3. Discussion

Degradation under constant one-sun illumination at comparable temperatures was fastest at OC biasing and slower at SC and

MPP biasing (**Figure 6**d and Figure S6, Supporting Information). These results are in agreement with those of previous studies performed under continuous simulated one-sun illumination.[10,12,13,15,18,39]

Stress testing at varying illumination schemes and cell temperatures showed differences in degradation patterns at different bias conditions. The differences are manifested mainly in the dependence of the degradation rates on the illumination dose and intensity. The observed differences indicate that different degradation mechanisms are active at different bias conditions. We suggest the simultaneous presence of multiple degradation mechanisms at all degrading PSCs, with different mechanisms dominating at different bias conditions. Bias-affected degradation mechanisms may include ion migration, either within the perovskite active layer, "intrinsic,"[41–45] or between different cell layers, "extrinsic"[17,19–21,46,47]; trap charging and discharging[15]; and defect formation due to reactions involving accumulated charge carriers[12].

Fast initial degradation stages were observed at all bias conditions studied. We postulate that ion migration may be responsible for this initial fast degradation, as it may occur at all bias conditions, and fast ion migration was previously demonstrated in PSCs.[45,48–50] Ion migration was previously suggested to degrade the cell performance by modifying the interfacial space regions[13]: Forward biasing (MPP, OC) may reduce the interfacial fields which repel ion migration of the opposite charge into them, driven by concentration gradients. Therefore, forward bias
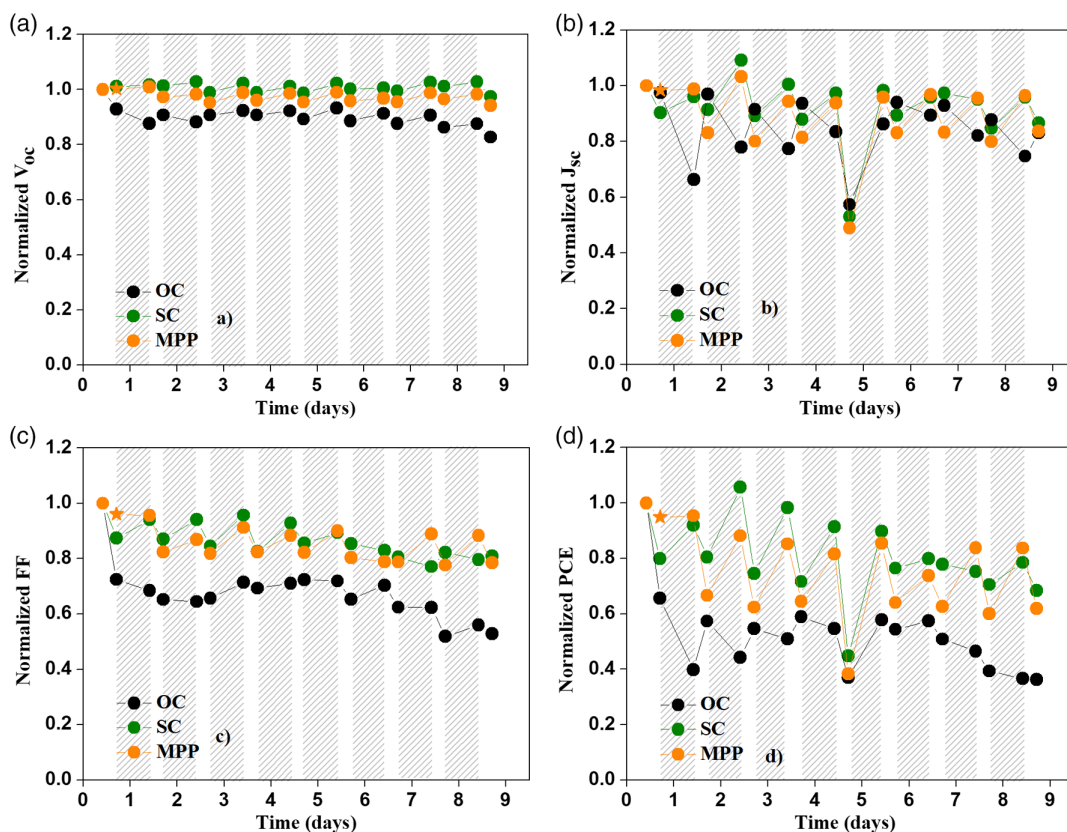

Figure 5. Variations of normalized PV parameters of PSCs ("Cell 1") as a function of outdoor exposure time under different biasing: a) V_{oc}, b) J_{sc}, c) FF, and d) PCE. Gray areas represent dark/ night-time periods.
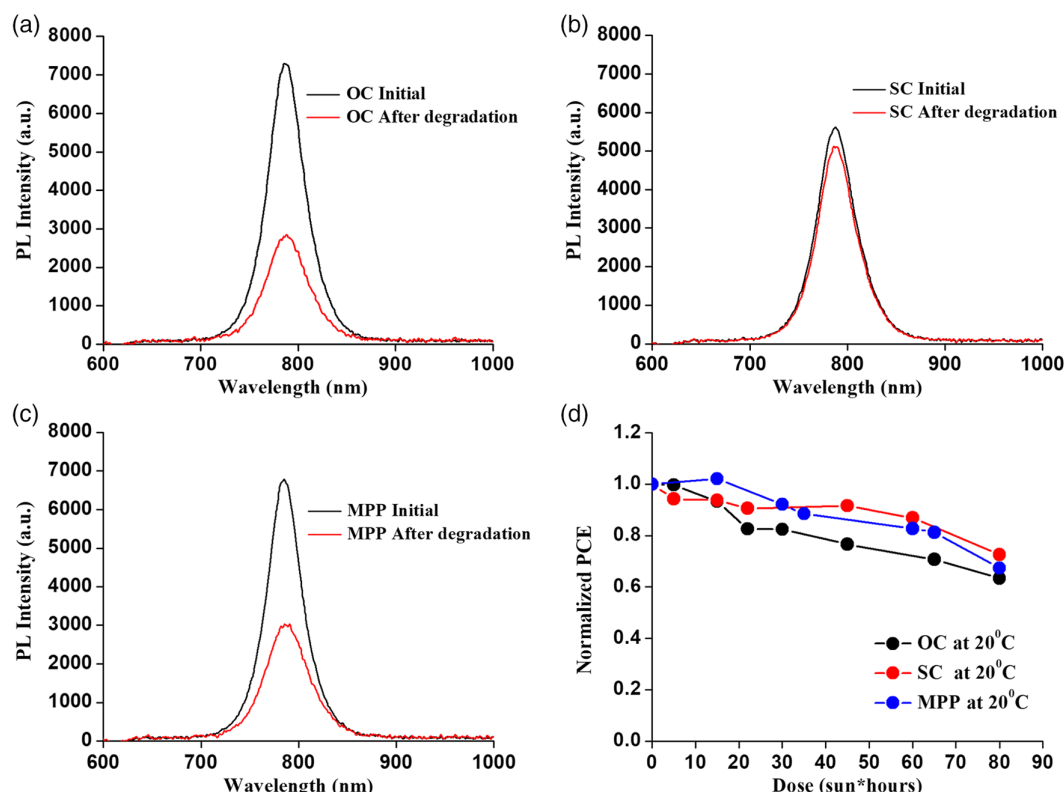
Figure 6. PL spectroscopy of PSCs ("Cell 3") stressed at one-sun-simulated illumination for 80 h at a) OC, b) SC, and c) MPP biasing. d) Normalized PCE variations with dose of the same cells used for PL measurements.

enhances such migration, decreasing the net charge and narrowing the space charge region(s), negatively affecting collection of photocurrents.[14] At SC, the opposite ion migration due to internal built-in electrical fields will widen these space charge regions causing a larger bias drop there, which will reduce the electric field in the bulk of the perovskite layer, negatively affecting photogenerated charge separation there.[8] As the mechanisms responsible for ion migration-induced degradation are different at different applied biases, the corresponding degradation may occur at different rates and amplitudes.

Intrinsic and extrinsic ion migration at SC conditions is driven by internal electric fields. The extent of degradation at SC conditions was found to depend on the light intensity during stressing (Figure 1b and 2c, Figure S3b, Supporting Information), which may be related to photogeneration of vacancies and other defects facilitating ion migration.[48,51] Therefore, this can be the dominant degradation mechanism for PSCs stressed at SC.[13] Additionally, enhanced ion migration at elevated temperatures, at larger illumination intensities, cannot be ruled out.

Accumulated illumination dose was found to control the extent of degradation at OC stressing (Figure 1a and 2b, Figure S3a, Supporting Information). It can therefore be assumed that an additional degradation mechanism is superimposed on the ion migration mechanism under OC stressing, whose extent is dose dependent. Such a mechanism may be defect formation by reaction with accumulated charges, causing the formation of traps enhancing recombination and degradation

of the PSC performance, in agreement with previous reports.[12,39] Indeed, enhanced nonradiative recombination may account for the observation that V_{oc} degradation and the related FF decrease were the dominant degrading parameters leading to PCE degradation under OC stressing (Figure S1, Supporting Information and Figure 5). Charge carriers are progressively generated and accumulated in the cell under OC biasing, as they are not extracted, and charge recombination rate is balanced by photogeneration ensuring constant electron concentration. Excess charge carriers-assisted trap formation pushes this balance to more carrier generation; therefore, the trap concentration further grows with illuminating dose.

PSCs stressed at MPP are expected to be affected by multiple mechanisms (ion diffusion, migration under internal fields, and trap formation); hence, their degradation shows both intensity and temperature dependence. However, as the driving forces for these mechanisms are reduced compared to OC conditions, the PCE degradation rate at MPP might be slower.

Photoluminescence (PL) spectroscopy provided support for this analysis, showing a significant decrease in PL intensity for cells stressed at OC or MPP, whereas SC stressing resulted in negligible changes in PL intensity (Figure 6a–c). PL peak position is not affected by light exposure, indicating that the signal originates from band-to-band radiative recombination in both fresh and degraded cells. The decrease in intensity may indicate the formation of traps, increasing nonradiative recombination.

4. Conclusion

In summary, we have studied the stability of encapsulated PSCs using concentrated sunlight, with independent control of sunlight intensity, cell temperature, and electrical bias during the exposure. Utilizing various light intensities afforded by sunlight concentration, as well as natural sunlight illumination, provided valuable information about factors affecting bias-dependent degradation, revealing different dominant mechanisms under different bias conditions.

We found that degradation of SC stressed cells depended mainly on light intensity with weaker dependence on the cell temperature or illuminating dose (intensity × time). This degradation is postulated to be due to intrinsic and extrinsic ion migration under internal electric fields, peaking at SC conditions. Ion migration driven by these internal fields is facilitated by photogenerated defects (e.g., vacancies), hence the dependence on light intensity during stressing.

Studies conducted at OC conditions revealed that PSC degradation mostly depended on illumination dose. Degradation at OC biasing may be explained by photogenerated radicals acting as charge traps, which are created via reaction with accumulated charge carriers, hence the dose dependence. Traps formation is supported by PL and V_{OC} decrease observed in OC biasing experiments. This mechanism is possibly accompanied by extrinsic ion diffusion that is not prevented by internal fields, which is dominant only at the earlier stages of degradation.

A combination of multiple mechanisms, all with reduced driving forces compared with OC/SC conditions, may explain observed degradation at MPP. The different dominant mechanisms at different stress conditions further stress the significance of stability studies at realistic operational bias (MPP for single-junction cells, possibly other bias conditions for tandems). Understanding the dominant degradation mechanism at relevant bias conditions can lead to methods to diminish or eliminate it.

5. Experimental Section

Device Fabrication: "Cell 1": ITO/SnO$_2$/Cs$_{0.15}$(CH(NH$_2$)$_2$)$_{0.85}$ PbI$_{2.75}$Br$_{0.25}$/Spiro-OMeTAD/Au, dual-cation perovskite cells were fabricated at TNO, Solliance, the Netherlands, with active device area of 0.16 cm^2. Glass substrates of 3 × 3 cm^2 with patterned ITO electrodes were purchased from Naranjo. The substrates were cleaned by sequential sonication in a detergent solution, deionized water, and isopropanol. The substrates were then treated with UV ozone for 30 min. Tin oxide (SnO$_2$) nanoparticle solution (15 wt%) purchased from Alfa Aesar was diluted by water in a volume ratio of 1:5. Spin coating of SnO$_2$ solution on glass/ITO substrates was performed with a spin speed of 2800 rpm for 50 s and annealed for 30 min at 150 °C. The resulting thickness of the SnO$_2$ layer was 30–40 nm. After the preparation of SnO$_2$, samples were transferred to a N$_2$-filled glove box for perovskite deposition.

The perovskite precursor solution was prepared by dissolving 8.259 g of lead iodide (PbI$_2$) (TCI), 2.85 g of formadiniu iodide (FAI) (GreatCell Solar), 0.895 g of lead bromide (PbBr$_2$) (TCI), and 0.112 g of cesium iodide (CsI) (Sigma Aldrich) in 4.5 mL of dimethyl formamide (DMF) and 0.5 mL of dimethyl sulfoxide (DMSO). The solution was stirred overnight at room temperature. The resulting solution was spin coated onto SnO$_2$-coated substrate at 2000 rpm (acceleration of 200 rpm s^{-1}) for 10 s followed by 5000 rpm (acceleration of 2000 rpm s^{-1}) for 30 s. During spin coating, 300 μL of antisolvent (chlorobenzene) was dropped onto substrate 20 s

prior to the end of the program. Samples were transferred to a hotplate for annealing at 100 °C for 30 min, resulting in a perovskite layer of 600 nm.

The 2,2',7,7'-tetrakis-(N,N-di-4-methoxyphenylamino)-9,9'-spirofluorine (Spiro-OMeTAD) solution (80 mg of Spiro-OMeTAD (Lumtec), 28 μL of 4-tert-butylpyridine, 17.5 μL of a 520 mg mL^{-1} LiN(CF$_3$SO$_2$)$_2$N solution in acetonitrile, and 20 μL of a 500 mg mL^{-1} FK209 cobalt salt in acetonitrile were added to 1 mL of chlorobenzene) was spin coated in air at 2000 rpm for 60 s onto the perovskite film and resulted in the formation of a 200 nm-thick hole-transporting layer. The complete Spiro-OMeTAD oxygen doping was attained by exposing the substrates to air under controlled humidity (RH = 48%) for additional 30 min. Subsequently, the substrates were transferred to the thermal evaporator under the pressure of 1.0 × 10^{-6} mbar, where 100 nm of Au back electrode was deposited on top of the Spiro-OMeTAD film. During the Au evaporation, a shadow mask was placed on each substrate, where the overlap between the ITO and Au electrodes determined the active device area of 0.16 cm^2. Encapsulation of the devices was performed by lamination of the barrier film (R2R manufactured at Holst Centre) with a pressure-sensitive adhesive, as published in a previous study.[52] The edges of the substrate were cleaned from the materials to ensure proper adhesion of the barrier film to the glass substrate at the edge and thereby prevent delamination and slow down the side ingress of water and oxygen.

"Cell 2": FTO/c-TiO$_2$/mp-TiO$_2$/Cs$_{0.2}$FA$_{0.8}$Pb(I$_{0.8}$Br$_{0.2}$)$_3$/Spiro/Au cells were fabricated at Hebrew University of Jerusalem (HUJI), with active device area of 0.14 cm^2. Patterned FTO glass substrates (15 Ω cm^{-1}, Pilkington) were cleaned by soap for 60 min followed by sonication in isopropanol and a mixture of ethanol and acetone for 15 min each. The substrates were then treated by UV ozone for 5 min to remove organic residues. A compact TiO$_2$ layer was prepared on the FTO substrates by spin coating a solution containing 200 μL titanium diisopropoxidebis (TiDIP, 75% isopropanol, Aldrich) diluted in 1.5 mL ethanol (Absolute >99%, Aldrich) at 5000 rpm for 30 s followed by annealing at 450 °C for 30 min. The consequent mesoporous TiO$_2$ layer was made using NR-30D paste (GreatCell Solar) diluted with ethanol (1:6 wt%) and spun at 5000 rpm for 30 s. The sample was then gradually heated to 500 °C for 30 min and cooled down to 100 °C. TiCl$_4$ treatment was made by soaking the sample in a bath containing 0.5 mL titanium chloride solution (5 M, Wako) in 50 mL triply distilled water for 30 min at 70 °C and annealing at 450 °C for 30 min. The substrates were placed into the glove box at 150 °C for perovskite deposition.

A 1.25 M solution of Cs$_{0.2}$FA$_{0.8}$Pb(I$_{0.8}$Br$_{0.2}$)$_3$ was prepared by dissolving stoichiometric amounts of CsI, PbBr$_2$, PbI$_2$ (Aldrich), and FAI (Dyesol) in a mixture of 825 μL anhydrous DMF and 175 μL DMSO (Aldrich). The solution was vortex mixed for few minutes until it was clear and stored at 65 °C for 4 h before use. The deposition of the perovskite layer was made by spin coating 50 μL of the perovskite solution on the prepared samples at 1000 rpm for 10 s followed by 5000 rpm for 30 s. At 15 s before the end of the program, 100 μL of chlorobenzene (Aldrich) was dripped on the substrate to form a light brown color perovskite film. The perovskite-coated substrates were then annealed at 100 °C for 40 min, changing their color to dark brown. After cooling down to room temperature, the hole-transport layer was formed by spin coating at 4000 rpm for 30 s a solution containing 0.036 g of spiro-OMeTAD in 500 μL chlorobenzene and adding 8.75 μL of bis(trifluoromethane)sulfonimide lithium salt in acetonitrile (520 mg mL^{-1}) and 14.4 μL of 4-tert- butilpyridine. A 70 nm-thick Au metallic back contact was thermally evaporated at a rate of 1.1 Å s^{-1} under pressure of 5×10^{-5} Torr.

For encapsulation, first the edges of the device were physically removed using a razor blade. A frame of Surlyn polymer (Meltonix 1170-60, Solaronix) was cut manually to fit the size of device. The polymer frame was placed on top of the device followed by a thin cover glass. A soldering pen was used (250 °C) to melt the polymer and glue the glass to the exposed substrate edges for complete sealing. Encapsulation was performed under nitrogen atmosphere in the glove box. The glass edges were then sealed with Torr Seal epoxy resin (Agilent Technologies).

"Cell 3": ITO/SnO2/Cs$_{0.05}$((CH$_3$NH$_3$)$_{0.15}$(CH(NH$_2$)$_2$)$_{0.85}$)$_{0.95}$PbI$_{2.55}$ Br$_{0.45}$/Spiro-OMeTAD/Au, triple-cation perovskite cells were fabricated

at TNO, Solliance, the Netherlands. Glass substrates were prepared as described for "Cell1".

First, 1.3 mM of PbI$_2$ (TCI) and 1.17 mM of FAI (GreatCell Solar) were dissolved in 1 mL DMF:DMSO solution (volume ratio of 9:1). Then, 1.3 mM

Figure 7. Illuminating Spectrum of AAA class Oriel Verasol LSS-7120 solar simulator used in this study.

of PbBr$_2$ (TCI) and 1.3 mM of methylammonium bromide (MABr) (GreatCell Solar) were dissolved in 1 mL of DMF:DMSO solution (volume ratio of 9:1). CsI (Sigma Aldrich) was dissolved in pure DMSO, adding 1.5 mM to 1 mL of solvent. The three solutions were stirred for at least 60 min before use. Then the three solutions were mixed together, to fabricate the mixed-cation, mixed-halide perovskite phase Cs$_{0.05}$(MA$_{0.15}$FA$_{0.85}$)$_{0.95}$PbI$_{2.55}$Br$_{0.45}$. The resulting solution was spin casted for 10 s at 1000 rpm and at 5000 rpm for 50 s onto a SnO$_2$-coated substrate. At the 40th second of the spin-coating process, 210 μL of an antisolvent (chlorobenzene) was dropped onto the substrate. Samples were transferred to a hotplate for annealing at 100 °C for 30 min, resulting in a 500 nm-thick perovskite layer. Further cell processing was done as described for "Cell 1".

Current Density–Voltage (J–V) Measurements: J–V characteristics were obtained using a Keithley 2401 source meter unit under the illumination of an AAA class oriel Verasol LSS-7120 solar simulator (light intensity of 67 mW cm^{-2}, **Figure 7**) with no temperature control. Reverse sweeps were performed from 1.2 to −0.2 V and forward sweeps from −0.2 to 1.2 V at a scan rate of 40 mV s^{-1}. As all described trends for forward and reverse sweeps were found to be similar, therefore, only the results from reverse sweeps are shown in the article.

Initial Cell Performance: "Cell 1" PSCs had an initial PCE of 14.9 ± 0.6%, $V_{oc} = 1097.9 ± 6.9$ mV, $J_{sc} = 13.8 ± 0.1$ mA cm^{-2}, and FF = 62.7 ± 3.8% in reverse scans. Typical J–V curves and average initial PCE of the cells are shown in **Figure 8**a,b, top panels. The cells were characterized at room temperature. No preconditioning was applied before the measurements.

Initial PCE of "Cell 2" PSCs was 13.4 ± 1.0%, $V_{oc} = 974.5 ± 30.5$ mV, $J_{sc} = 13.4 ± 0.5$ mA cm^{-2}, and FF = 52.4 ± 9.8% in reverse scans.
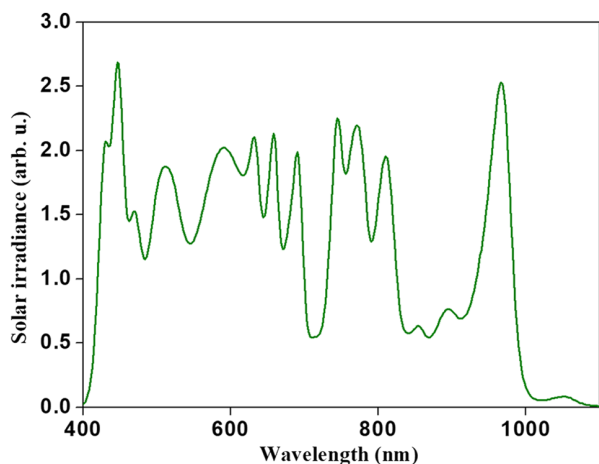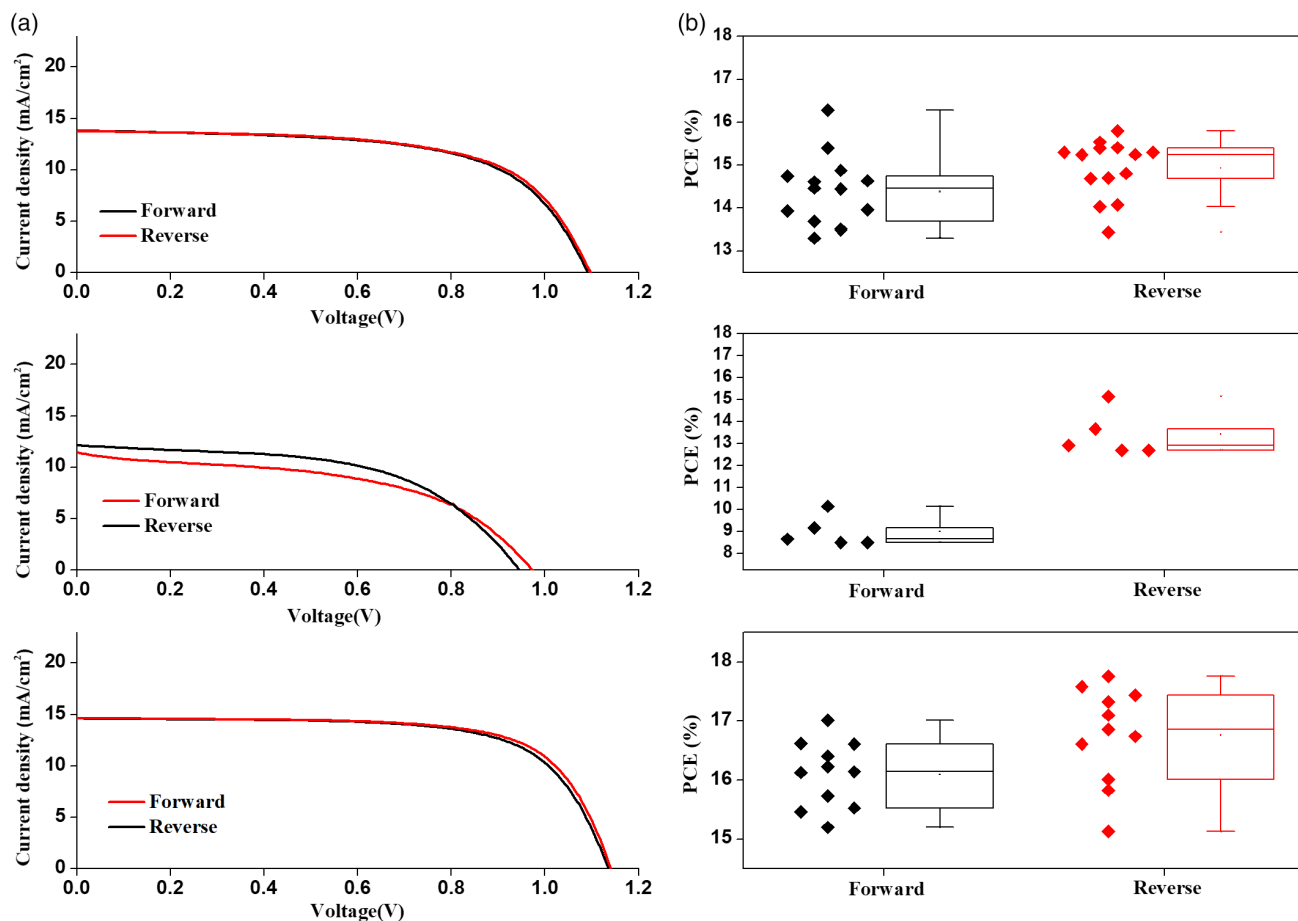

Figure 8. a) Typical J–V scans of the cells under study; b) average PCE values of the devices used, top: "Cell 1", middle: "Cell 2", bottom "Cell 3". Note that the J–V curves were obtained under simulated solar illumination of intensity 67 mW cm^{-2}.

Typical J–V curves and average initial PCE of the cells are shown in Figure 8a,b, middle panels. The cells were tested at room temperature with a preconditioning time of 45 s under the solar simulator illumination.

Initial PCE of "Cell 3" PSCs was $16.8 \pm 0.8\%$, $V_{oc} = 1137.7 \pm 6.2$ mV, $J_{sc} = 14.6 \pm 0.4$ mA cm^{-2}, and FF $= 67.6 \pm 2.1\%$. Typical J–V curves and average initial PCE of the cells are shown in Figure 8a,b, bottom panels. The cells were tested at room temperature with no preconditioning.

Small sample-to-sample variations did not result in obvious changes in the degradation trends; therefore, the parameter variations with stressing are shown in the article as normalized by the initial value for clarity.

Cell Stressing: All experiments were performed in Sede Boqer, Israel (Lat. 30.8°N, Lon. 34.8°E, Alt. 475 m). The sunlight spectrum measured at noontime ± 2–3 h in Sede Boqer is very close to the AM1.5G spectrum.[53] Each stress test, represented by one data point in Section 2, was repeated 1–3 times with different devices (total of over 50 devices), with no significant changes in the results. The measurement error was estimated as 5% of the measured value, derived from estimated variations in the measured illumination intensity.

Natural sunlight was concentrated using two home-made systems: 1) In the "mini-dish" setup,[54] sunlight was concentrated by a paraboloidal mirror. The setup was mounted on a dual-axis tracker. The concentrated sunlight was focused onto a flat mirror which reflects it into a 1 mm-diameter optical fiber, which delivered the concentrated sunlight to the indoor lab. Pizza-slice iris was used to modulate the intensity of the incoming light. A 0.25 cm^2 cross-section kaleidoscope was placed between the distal fiber tip and the perovskite sample to achieve flux uniformity. The sample was placed on top of a water-cooled plate in which the temperature was set to 20 °C. A side fan was used to prevent humidity condensation on the sample. Initially (OC and SC biasing, Figure 2 and Figure S1–S3, Supporting Information), the cells were placed in a plastic holder on top of the cooling plate, which lowered the cooling efficiency. Later (MPP biasing, Figure 4), the cooling efficiency was improved by placing the cells on a copper plate on the cooling stage for improved thermal conductance, which resulted in lower cell temperatures. 2) The "solar furnace"[55] consists of a dual-axis tracking flat heliostat that reflects sunlight into the laboratory. A flat mirror (with a hole at its center) tilted at 45° redirects the light toward a 526 mm-diameter paraboloidal dish, whose focal plane is behind the hole in the tilted mirror. A mechanical shutter between the heliostat and the flat mirror was used to modulate the light intensity. A kaleidoscope (with cross-section area 0.16 cm^2) was used to achieve flux uniformity. A mechanical chopper (50% open area) was used to effectively control the cell temperature during illumination. Light chopping enables effective heat dissipation during the nonirradiated periods of the chopper cycles.[31,32,56] Exposure doses in this setup were calculated taking into account light chopping (the exposure time was the overall stress time divided by two).

A pyrometer (Nova II display, Ophir, with 5% accuracy) was used to measure the incident power of concentrated sunlight in both the above-mentioned techniques. A T-type thermocouple was fixed to the transparent substrate of the solar cell near the exposed area to read the cell temperature. All temperature readings were taken after few minutes of waiting, when the readings showed stable values.

For outdoor stressing, the devices were exposed to natural sunlight during daytime (from 10:00 to 17:00) and kept in the dark in a glove box for the rest of the day. PSCs were stressed on a dual-axis sun-tracking platform, which ensured that impinging radiation was close to 1 sun (100 mW cm^{-2}). PV performance variations were characterized via J–V curves measured using the solar simulator twice per day, in the morning and evening, as described earlier. The PSC under MPP biasing was incidentally covered on the first day of outdoor exposure, hence the star symbol in Figure 5.

Stressing under simulated one-sun illumination was applied using the SolarConstant MHG 4000/2500 solar simulator (K.H. Steuernagel Lichttechnik GmbH) equipped with a metal halide lamp, which produces a continuous spectrum close to the natural sunlight (**Figure 9**), with illumination intensity of 100 mW cm^{-2}. Due to the significant IR illumination of this simulator, the cells were placed on a water-cooled platform set to
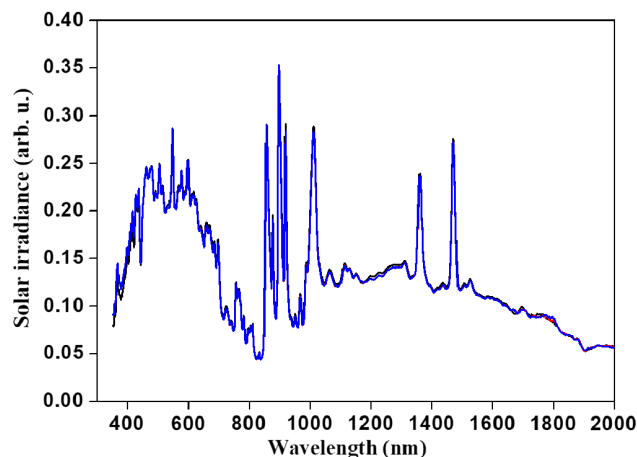

Figure 9. Illuminating spectrum of B class SolarConstant MHG 4000/2500 solar simulator.

20 °C with a side fan for temperature control. The cell temperature during stressing was 25 ± 1 °C.

SC conditions were achieved by connecting the two contacts of the PSC using a metal wire glued to both electrodes with silver paste. MPP tracking was performed by a Candlelight® system. The tracker algorithm is described in a previous study.[57] MPP biasing during outdoor exposure was applied using a home-made resistor setup with a perturb-and-observe methodology.

PL Spectroscopy: PL spectroscopy utilized an in-house built system.[32] Excitation at 600 nm was afforded by a supercontinuum laser (Fianium Whitelase, Model-WL-SC-400-40) filtered by an acousto-optic tunable filter system (Fianium, AOTF). Aluminum mirrors guided the filtered laser light to a filter cube (Thorlabs, DFM1) which contained a dichroic beam splitter (Semrock, FF625-SDi01-25x36) and a shortpass filter (Semrock, FF01-650/SP-25). The excitation beam was focused by an objective lens (40 X/NA 0.7) onto the sample, and the intensity at the sample was ≈167 mW cm^{-2}. The same objective lens collected the PL, filtered by a longpass filter (Semrock, FF01-685/LP-25) and coupled via an optical fiber to a concave-grating spectrometer (Stellar Net Inc-model- BLK-C-SR). All PL measurements were applied to PSCs at OC. PL intensity was found to be relatively stable under the excitation laser beam; thus, Figure 5 shows instantaneously recorded spectra.

Supporting Information

Supporting Information is available from the Wiley Online Library or from the author.

Conflict of Interest

The authors declare no conflict of interest.

[1] NREL, Best Research-Cell Efficiency Chart | Photovoltaic Research, https://www.nrel.gov/pv/cell-efficiency.html (accessed: September 2019).

[2] R. Wang, M. Mujahid, Y. Duan, Z.-K. Wang, J. Xue, Y. Yang, *Adv. Funct. Mater.* **2019**, 1808843, https://doi.org/10.1002/adfm.201808843.

[3] F. Lang, O. Shargaieva, V. V. Brus, H. C. Neitzert, J. Rappich, N. H. Nickel, *Adv. Mater.* **2018**, *30*, 1702905.

[4] S.-W. Lee, S. Kim, S. Bae, K. Cho, T. Chung, L. E. Mundt, S. Lee, S. Park, H. Park, M. C. Schubert, S. W. Glunz, Y. Ko, Y. Jun, Y. Kang, H.-S. Lee, D. Kim, *Sci. Rep.* **2016**, *6*, 38150.

[5] A. A. Melvin, V. D. Stoichkov, J. Kettle, D. Mogilyansky, E. A. Katz, I. Visoly-Fisher, *Sol. Energy* **2018**, *159*, 794.

[6] P. Yadav, D. Prochowicz, E. A. Alharbi, S. M. Zakeeruddin, M. Grätzel, *J. Mater. Chem. C* **2017**, *5*, 7799.

[7] N.-K. Kim, Y. H. Min, S. Noh, E. Cho, G. Jeong, M. Joo, S.-W. Ahn, J. S. Lee, S. Kim, K. Ihm, H. Ahn, Y. Kang, H.-S. Lee, D. Kim, *Sci. Rep.* **2017**, *7*, 4645.

[8] J. A. Schwenzer, L. Rakocevic, R. Gehlhaar, T. Abzieher, S. Gharibzadeh, S. Moghadamzadeh, A. Quintilla, B. S. Richards, U. Lemmer, U. W. Paetzold, *ACS Appl. Mater. Interfaces* **2018**, *10*, 16390.

[9] R. K. Misra, S. Aharon, B. Li, D. Mogilyansky, I. Visoly-Fisher, L. Etgar, E. A. Katz, *J. Phys. Chem. Lett.* **2015**, *6*, 326.

[10] D. Bryant, N. Aristidou, S. Pont, I. Sanchez-Molina, T. Chotchunangatchaval, S. Wheeler, J. R. Durrant, S. A. Haque, *Energy Environ. Sci.* **2016**, *9*, 1655.

[11] J. M. Howard, E. M. Tennyson, S. Barik, R. Szostak, E. Waks, M. F. Toney, A. F. Nogueira, B. R. A. Neves, M. S. Leite, *J. Phys. Chem. Lett.* **2018**, *9*, 3463.

[12] K. Domanski, E. A. Alharbi, A. Hagfeldt, M. Grätzel, W. Tress, *Nat. Energy* **2018**, *3*, 61.

[13] M. V. Khenkin, A. K. M. E. A. Katz, I. Visoly-Fisher, *Energy Environ. Sci.* **2019**, *12*, 550.

[14] S. Bae, S. Kim, S.-W. Lee, K. J. Cho, S. Park, S. Lee, Y. Kang, H.-S. Lee, D. Kim, *J. Phys. Chem. Lett.* **2016**, *7*, 3091.

[15] W. Nie, J.-C. Blancon, A. J. Neukirch, K. Appavoo, H. Tsai, M. Chhowalla, M. A. Alam, M. Y. Sfeir, C. Katan, J. Even, S. Tretiak, J. J. Crochet, G. Gupta, A. D. Mohite, *Nat. Commun.* **2016**, *7*, 11574.

[16] A. R. Bowring, L. Bertoluzzi, B. C. O'Regan, M. D. McGehee, *Adv. Energy Mater.* **2018**, *8*, 1702365.

[17] J. P. Bastos, U. W. Paetzold, R. Gehlhaar, W. Qiu, D. Cheyns, S. Surana, V. Spampinato, T. Aernouts, J. Poortmans, *Adv. Energy Mater.* **2018**, *8*, 1800554.

[18] T. Duong, H. K. Mulmudi, Y. Wu, X. Fu, H. Shen, J. Peng, N. Wu, H. T. Nguyen, D. Macdonald, M. Lockrey, T. P. White, K. Weber, K. Catchpole, *ACS Appl. Mater. Interfaces* **2017**, *9*, 26859.

[19] Z. Li, C. Xiao, Y. Yang, S. P. Harvey, D. H. Kim, J. A. Christians, M. Yang, P. Schulz, S. U. Nanayakkara, C.-S. Jiang, J. M. Luther, J. J. Berry, M. C. Beard, M. M. Al-Jassim, K. Zhu, *Energy Environ. Sci.* **2017**, *10*, 1234.

[20] K. Domanski, J.-P. Correa-Baena, N. Mine, M. K. Nazeeruddin, A. Abate, M. Saliba, W. Tress, A. Hagfeldt, M. Grätzel, *ACS Nano* **2016**, *10*, 6306.

[21] H. J. Jung, D. Kim, S. Kim, J. Park, V. P. Dravid, B. Shin, *Adv. Mater.* **2018**, *30*, 1802769.

[22] C. Besleaga, L. E. Abramiuc, V. Stancu, A. G. Tomulescu, M. Sima, L. Trinca, N. Plugaru, L. Pintilie, G. A. Nemnes, M. Iliescu, H. G. Svavarsson, A. Manolescu, I. Pintilie, *J. Phys. Chem. Lett.* **2016**, *7*, 5168.

[23] Y. Zhao, W. Zhou, H. Tan, R. Fu, Q. Li, F. Lin, D. Yu, G. Walters, E. H. Sargent, Q. Zhao, *J. Phys. Chem. C* **2017**, *121*, 14517.

[24] W. Tress, M. Yavari, K. Domanski, P. Yadav, B. Niesen, J. P. Correa Baena, A. Hagfeldt, M. Graetzel, *Energy Environ. Sci.* **2018**, *11*, 151.

[25] S. G. Motti, M. Gandini, A. J. Barker, J. M. Ball, A. R. Srimath Kandada, A. Petrozza, *ACS Energy Lett.* **2016**, *1*, 726.

[26] G. Y. Kim, A. Senocrate, T.-Y. Yang, G. Gregori, M. Grätzel, J. Maier, *Nat. Mater.* **2018**, *17*, 445.

[27] S. T. Birkhold, J. T. Precht, H. Liu, R. Giridharagopal, G. E. Eperon, L. Schmidt-Mende, X. Li, D. S. Ginger, *ACS Energy Lett.* **2018**, *3*, 1279.

[28] T. Handa, D. M. Tex, A. Shimazaki, T. Aharen, A. Wakamiya, Y. Kanemitsu, *Opt. Express* **2016**, *24*, A917.

[29] A. J. Pearson, G. E. Eperon, P. E. Hopkinson, S. N. Habisreutinger, J. T.-W. Wang, H. J. Snaith, N. C. Greenham, *Adv. Energy Mater.* **2016**, *6*, 1600014.

[30] E. A. Katz, I. Visoly-Fisher, D. Feuermann, R. Tenne, J. M. Gordon, *Adv. Mater.* **2018**, *30*, 1800444.

[31] I. Visoly-Fisher, A. Mescheloff, M. Gabay, C. Bounioux, L. Zeiri, M. Sansotera, A. E. Goryachev, A. Braun, Y. Galagan, E. A. Katz, *Sol. Energy Mater. Sol. Cells* **2015**, *134*, 99.

[32] R. Guo, M. V. Khenkin, G. E. Arnaoutakis, N. A. Samoylova, J. Barbé, H. K. H. Lee, W. C. Tsoi, E. A. Katz, *Sol. RRL* **2019**, 1900270, https://doi.org/10.1002/solr.201900270.

[33] C. Law, L. Miseikis, S. Dimitrov, P. Shakya-Tuladhar, X. Li, P. R. F. Barnes, J. Durrant, B. C. O'Regan, *Adv. Mater.* **2014**, *26*, 6268.

[34] Z. Wang, Q. Lin, B. Wenger, M. G. Christoforo, Y.-H. Lin, M. T. Klug, M. B. Johnston, L. M. Herz, H. J. Snaith, *Nat. Energy* **2018**, *3*, 855.

[35] J. P. Bastos, G. Uytterhoeven, W. Qiu, U. W. Paetzold, D. Cheyns, S. Surana, J. Rivas, M. Jaysankar, W. Song, T. Aernouts, J. Poortmans, R. Gehlhaar, *ACS Appl. Mater. Interfaces* **2019**, *11*, 16517.

[36] A. D. Sheikh, R. Munir, M. A. Haque, A. Bera, W. Hu, P. Shaikh, A. Amassian, T. Wu, *ACS Appl. Mater. Interfaces* **2017**, *9*, 35018.

[37] T. Duong, Y. Wu, H. Shen, J. Peng, S. Zhao, N. Wu, M. Lockrey, T. White, K. Weber, K. Catchpole, *Sol. Energy Mater. Sol. Cells* **2018**, *188*, 27.

[38] G. Abdelmageed, C. Mackeen, K. Hellier, L. Jewell, L. Seymour, M. Tingwald, F. Bridges, J. Z. Zhang, S. Carter, *Sol. Energy Mater. Sol. Cells* **2018**, *174*, 566.

[39] B. Chen, J. Song, X. Dai, Y. Liu, P. N. Rudd, X. Hong, J. Huang, *Adv. Mater.* **2019**, *31*, 1902413.

[40] M. V. Khenkin, A. K. M. I. Visoly-Fisher, S. Kolusheva, Y. Galagan, F. Di Giacomo, O. Vukovic, B. R. Patil, G. Sherafatipour, V. Turkovic, H.-G. Rubahn, M. Madsen, A. V. Mazanik, E. A. Katz, *ACS Appl. Energy Mater.* **2018**, *1*, 799.

[41] C. Ran, J. Xu, W. Gao, C. Huang, S. Dou, *Chem. Soc. Rev.* **2018**, *47*, 4581.

[42] Q. Jeangros, M. Duchamp, J. Werner, M. Kruth, R. E. Dunin-Borkowski, B. Niesen, C. Ballif, A. Hessler-Wyser, *Nano Lett.* **2016**, *16*, 7013.

[43] M. Bag, L. A. Renna, R. Y. Adhikari, S. Karak, F. Liu, P. M. Lahti, T. P. Russell, M. T. Tuominen, D. Venkataraman, *J. Am. Chem. Soc.* **2015**, *137*, 13130.

[44] M. H. Du, *J. Mater. Chem. A* **2014**, *2*, 9091.

[45] T.-Y. Yang, G. Gregori, N. Pellet, M. Grätzel, J. Maier, *Angew. Chem., Int. Ed.* **2015**, *54*, 7905.

[46] W. Ming, D. Yang, T. Li, L. Zhang, M.-H. Du, *Adv. Sci.* **2018**, *5*, 1700662.

[47] E. Bi, H. Chen, F. Xie, Y. Wu, W. Chen, Y. Su, A. Islam, M. Grätzel, X. Yang, L. Han, *Nat. Commun.* **2017**, *8*, 15330.

[48] J. Xing, Q. Wang, Q. Dong, Y. Yuan, Y. Fang, J. Huang, *Phys. Chem. Chem. Phys.* **2016**, *18*, 30484.

[49] D. Yang, W. Ming, H. Shi, L. Zhang, M.-H. Du, *Chem. Mater.* **2016**, *28*, 4349.

[50] Z. Xiao, Y. Yuan, Y. Shao, Q. Wang, Q. Dong, C. Bi, P. Sharma, A. Gruverman, J. Huang, *Nat. Mater.* **2014**, *14*, 193.

[51] C. Peng, J. Chen, H. Wang, P. Hu, *J. Phys. Chem. C* **2018**, *122*, 27340.

[52] P. van de Weijer, P. C. P. Bouten, S. Unnikrishnan, H. B. Akkerman, J. J. Michels, T. M. B. van Mol, *Org. Electron.* **2017**, *44*, 94.

[53] D. Berman, D. Faiman, *Sol. Energy Mater. Sol. Cells* **1997**, *45*, 401.

[54] E. A. Katz, J. M. Gordon, W. Tassew, D. Feuermann, *J. Appl. Phys.* **2006**, *100*, 044514.

[55] J. M. Gordon, D. Babai, D. Feuermann, *Sol. Energy Mater. Sol. Cells* **2011**, *95*, 951.

[56] A. Braun, B. Hirsch, A. Vossier, E. A. Katz, J. M. Gordon, *Prog. Photovoltaics: Res. Appl.* **2013**, *21*, 202.

[57] N. Pellet, F. Giordano, M. Ibrahim Dar, G. Gregori, S. M. Zakeeruddin, J. Maier, M. Grätzel, *Prog. Photovoltaics: Res. Appl.* **2017**, *25*, 942.